

0° to 60°. The small variations in performance produced by these changes suggests that an ejector with a similar configuration offers good possibilities for use as an augmentor flap on the trailing edge of a conventional wing. Such an application is illustrated in Fig. 13.

Conclusions

Analysis has shown that the thrust augmentation of compact aircraft ejectors can be increased by accelerating the rate of entrainment by the primary jet. This has been accomplished with a nozzle which produces a series of streamwise vortices in the jet discharge. Tests of a simple ejector employing these nozzles have shown a significant improvement in the level of augmentation.

The effect of hypermixing is not to improve ejector performance by minimizing losses. In fact, the lower efficiency of hypermixing nozzles is a penalty that must be paid for their use. However, by assuring more nearly complete mixing of the flow in a shorter distance, it becomes possi-

ble to diffuse the flow efficiently and consequently obtain higher net levels of augmentation.

References

- ¹Bevilaqua, P. M. and Lykoudis, P. S., "Mechanism of Entrainment in Turbulent Wakes," *AIAA Journal*, Vol. 9, No. 8, Aug. 1971, pp. 1657-1659.
- ²Bevilaqua, P. M., "An Eddy Viscosity Model for Hypermixing Jets and Wakes," Rept. AD 743-297, April 1972, Aerospace Research Labs., Wright-Patterson Air Force Base, Ohio.
- ³Fancher, R. B., "Low Area Ratio, Thrust Augmenting Ejectors," *Journal of Aircraft*, Vol. 9, No. 3, March 1972, pp. 243-248.
- ⁴von Karman, T., "Theoretical Remarks on Thrust Augmentation," *Reissner Anniversary Volume*, Edwards Bros., Ann Arbor, Mich., 1949, pp. 461-468.
- ⁵Quinn, B. P., "Compact Ejector Thrust Augmentation," *Journal of Aircraft*, Vol. 10, No. 8, Aug. 1973, pp. 481-486.
- ⁶Viets, H., "The Three-Dimensional Laminar Elliptical Jet in a Coflowing Stream," Rept. AD 754-227, Dec. 1972, Aerospace Research Labs., Wright-Patterson Air Force Base, Ohio.
- ⁷Prandtl, L., "Attaining a Steady Air Stream in Wind Tunnels," TM 726, Oct. 1933, NACA.

JUNE 1974

J. AIRCRAFT

VOL. 11, NO. 6

Integrated Airframe-Nozzle Performance for Designing Twin-Engine Fighters

E. R. Glasgow*

Lockheed-California Company, Burbank, Calif.

Performance data for designing fighter aircraft having twin buried engines and dual nozzles were obtained from an experimental investigation of over 200 large-scale, twin-nozzle/aftbody configurations. Sufficient pressure and force balance data were obtained for exhaust nozzle pressure ratios within the operating range of a typical advanced technology engine to allow the effect of the following aft-end design variables to be determined: nozzle type, power setting position, axial position, solid body exhaust simulation, and lateral spacing; interfairing type, length, height, and base area; vertical stabilizer type, position, and rudder deflection; horizontal stabilizer deflection; and fuselage area distribution. In order to utilize the wind-tunnel data for predicting aircraft performance, the effects on aft-end drag of support system interference, inlet mass flow, lifting surface span reduction, and tunnel Reynolds number were also determined.

Nomenclature

A_{CC}	= nozzle cross-sectional area at F.S. 133.182, customer connect station
A_E	= nozzle exit area
A_{MB}	= aftbody boattail cross-sectional area at F.S. 113.188, metric break area
A_P	= stabilizer planar area
A_S	= nozzle shroud internal cross-sectional area at nozzle exit station
A_T	= nozzle throat area
A_W	= wing reference area, 2667.6 in. ²
A/B	= afterburning power setting
$C_{D(AE)}$	= aft-end drag coefficient—includes nozzle and aftbody fuselage and interfairing drag—based on nozzle axes and wing area, A_W
C_P	= pressure coefficient
D_{CC}	= maximum exposed nozzle diameter, 8 in.

F.S.	= fuselage station, longitudinal distance aft of a point 1.041 in. aft of model nose
L	= distance from customer connect station to trailing edge of interfairing or nozzle, inches
M_∞	= freestream Mach number
NPR	= nozzle pressure ratio (nozzle total/ambient static)
Re	= Reynolds number per foot
S/D	= nozzle lateral spacing ratio, distance between nozzle centerlines divided by D_{CC}
X	= distance
α	= interfairing upper surface trailing edge angle relative to nozzle centerline, degrees
β	= interfairing lower surface trailing edge angle relative to nozzle centerline, degrees
$\Delta C_{D(AE)}$	= aft-end drag coefficient increment due to strut interference effects

Introduction

THE achievement of proper airframe/nozzle integration has become significantly more difficult and important with the advent of the multimission aircraft requiring variable geometry nozzles to operate over a broad range of altitudes and Mach numbers. The mutual interactions that occur between the nozzle exhaust and the external flowfield can alter the pressure distributions on the aft-end of the fuselage and produce both internal and exter-

Presented as Paper 73-1303 at the AIAA/SAE 9th Propulsion Conference, Las Vegas, Nev., November 5-7, 1973; submitted November 26, 1973; revision received March 29, 1974. This work was sponsored by the Air Force Flight Dynamics Laboratory under Contracts F33657-70-C-0511 and F33615-72-C-1748.

Index categories: Aircraft Configuration Design; Aircraft Performance; Airbreathing Propulsion, Subsonic and Supersonic.

*Research Specialist, Member AIAA.

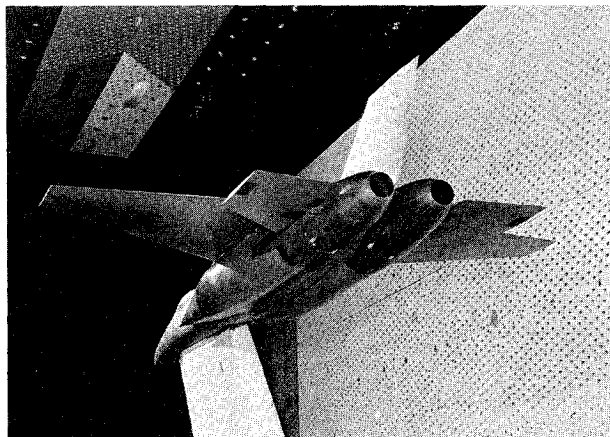


Fig. 1 Strut-supported model with faired-over inlets installed in AEDC 16-foot transonic propulsion wind tunnel.

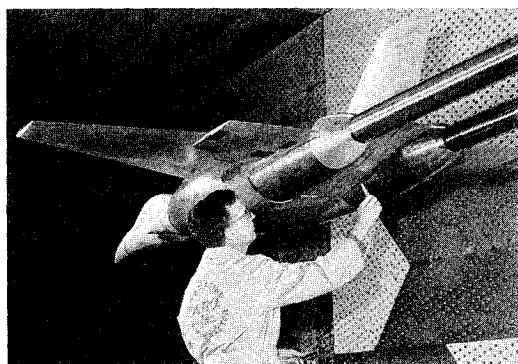


Fig. 2 Sting-supported model with faired-over inlets installed in AEDC 16-foot transonic propulsion wind tunnel.

nal flow separation. Such interactions can result in significant penalties in both aircraft drag and engine thrust. It has been difficult in the past to minimize these losses because adequate analytical methods and empirical information were not available during the aircraft design phase.

In order to improve this situation, a sixteen month program was initiated in 1972 for the development and assembly of design criteria and prediction techniques for producing improved twin-nozzle/afterbody installations.^{1,2} The results of this experimental and analytical effort are a direct extension of those obtained during a thirty-two month program initiated in 1969^{3,4} in which both isolated nozzle/afterbody configurations and twin-nozzle/afterbody configurations were examined. During the isolated nozzle model tests, large-scale (8-in. diam) convergent, convergent-divergent, and plug nozzles were investigated. During the twin-jet tests, the same nozzles were installed in a generalized model of an advanced air superiority fighter having twin buried engines and dual nozzles. An evaluation of analytical and empirical methods for predicting the thrust and drag of these nozzle configurations has been discussed previously.^{5,6}

The purpose of this paper is to present the experimental techniques and results associated with the twin-jet tests. A strut-supported jet-effects aircraft model with faired-over inlets and high pressure air for simulating the nozzle exhaust was used during the program to obtain the aft-end drag for a complete matrix of twin-nozzle/afterbody configurations. Sufficient jet-effects model data was obtained so that the results could be used in place of isolated model data during the early stages of aircraft design. To insure that the jet-effects model data is properly used in predicting aircraft performance, the effects on aft-end drag of support system interference, inlet mass flow, lift-

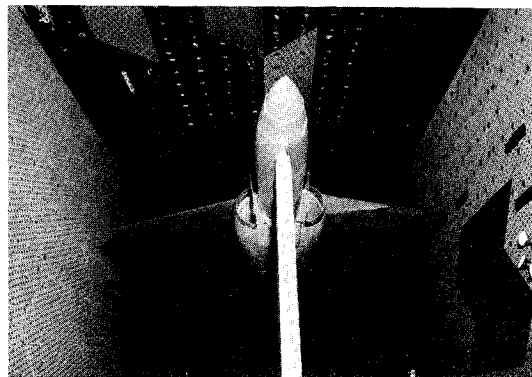


Fig. 3 Strut-supported model with flow-through inlets installed in AEDC 16-foot transonic propulsion wind tunnel.

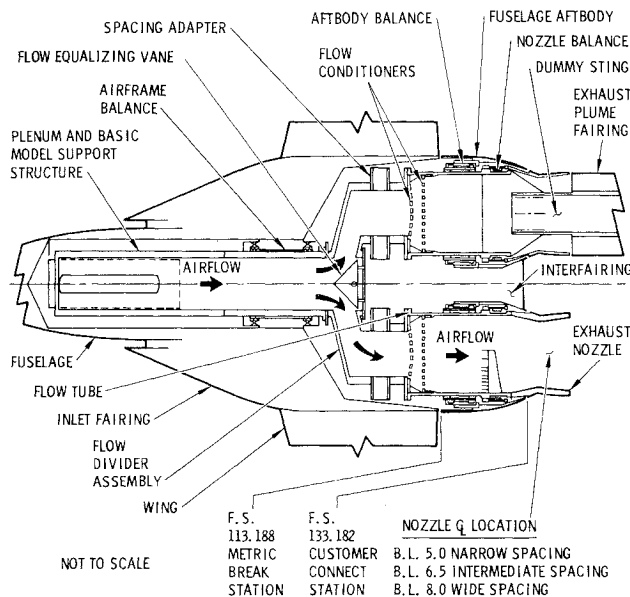


Fig. 4 Internal arrangement of strut-supported model with faired-over inlets.

ing surface span reduction, and tunnel Reynolds number were also determined.

Testing Techniques

The basic test configuration is a modified version of the A-2 twin-jet air superiority fighter design developed by General Dynamics under contract with the Air Force Flight Dynamics Laboratory.⁷ The wind-tunnel model is approximately 12 ft in length and has a wing span of 7.9 ft. All testing was conducted over a 0.6 to 2.5 Mach number range in the AEDC (Arnold Engineering Development Center) 16-foot PWT (Propulsion Wind Tunnel).

Model Arrangement

Three basic model internal arrangements were employed during the program: a strut-supported model with faired-over inlets (Fig. 1), a sting-supported model with faired-over inlets (Fig. 2), and a strut-supported model with flow-through inlets (Fig. 3). All model arrangements utilize five force balances (one airframe balance, two afterbody balances, and two nozzle balances) for determining the forces and moments exerted on the external model components. The internal model components function as the basic model support structure and are, therefore, non-metric.

A diagram of the general internal arrangement of the strut-supported model with faired-over inlets (i.e., jet-effects model) is shown in Fig. 4. For this arrangement, the

nozzle exhaust flow was simulated by either high-pressure nonheated air or by nonmetric dummy stings attached to the flow tubes. The entire flow tube and nozzle assembly was attached to a spacer adapter which could be positioned such that three nozzle lateral spacings could be investigated. Changes to the fuselage centerbody and interfairing were required in order to accommodate the different nozzle spacings.

For the flowing exhaust situation, high pressure air was metered within the tunnel plenum and supplied to the model through the support strut. It was divided within the model into two equal nozzle streams with the aid of a manually positioned flow equalizing vane. These streams then entered the flow tube and exhaust nozzle. For the dummy sting exhaust situation, the high-pressure air valve was closed and the nozzle inner shell was replaced with five-foot long dummy stings which have the same external contour as the load carrying stings.

The internal arrangement of the sting-supported model with faired-over inlets consisted of twin load-carrying nonmetric stings which extended through the nozzles (nozzle inner shell removed) and attached to the inner sleeve of the airframe balance. Two attachment plates were provided so that both narrow-spaced and wide-spaced configurations could be investigated. No high-pressure air was required to flow through the model since the nozzle exhaust plumes were simulated by attaching fairings to the load-carrying stings.

The internal arrangement of the strut-supported model with flow-through inlets consisted of open nosed inlets and associated boundary-layer diverters and transition sections between the inlet and flow tube for accommodating three nozzle lateral spacings. Internal flow restrictors were employed to vary the inlet mass flow and two-foot long nozzle extensions were used for most configurations in order to eliminate the effect of the nozzle exhaust flow on aft-end drag. A metric break was provided just inside the inlet cowl lip so that the airframe balance would measure only external forces.

Configuration Variables

Over 200 twin-nozzle/aftbody configurations, consisting of the following configuration variables, were examined during the program.

Nozzle type: convergent flap, convergent iris, convergent-divergent, convergent-divergent ejector, or unshrouded plug.

Nozzle throat area: 100% (maximum afterburning), 74% (partial afterburning), or 48% (normal power).

Nozzle axial position: nozzle fully or partially exposed to the external flowfield.

Nozzle exhaust simulation: high-pressure nonheated air or solid plume bodies.

Nozzle lateral spacing ratio: 1.25 (narrow), 1.625 (intermediate), or 2.0 (wide).

Interfairing type: horizontal wedge or vertical wedge.

Interfairing length: trailing edge located at -4.0, 0, 3.5, 8.216, or 13.0 in. aft of the customer connect station.

Interfairing height: trailing edge 1.8 in. above or along the nozzle centerline.

Interfairing base area: three interfairings.

Vertical stabilizer type: single or twin.

Vertical stabilizer position: forward or aft mounted single or vertical or canted twin.

Rudder deflection: 0, 4.0, 11.0, or -11.0°.

Horizontal stabilizer deflection: -0.4, -2.0, or -5.0°.

Fuselage shape: basic or alternate.

Inlet type: faired-over or flow-through.

Inlet mass flow ratio: three internal flow restrictors.

Wing: installed or replaced with fairing.

Vertical stabilizer area: 100% (full), 78% (partial), 40% (short), or zero (stabilizer removed).

Horizontal stabilizer area: 100% (full), 70% (partial), 24% (short), or zero (stabilizer removed).

Aft Fuselage Fairing: basic, alternate, or removed.

Instrumentation

The instrumentation employed within the model and tunnel plenum consisted of one airframe balance, two aftbody balances, two nozzle balances, approximately 240 pressure taps, twelve thermocouples, one venturi meter, and one Swirlmeter. Four alternate balances (one airframe, one aftbody, and two nozzle) were available in the event of balance damage.

A six-component airframe balance was used to obtain the aerodynamic forces and moments on the horizontal and vertical stabilizers and all external model components forward of the wing trailing edge. Two six-components aftbody balances were used to obtain the aerodynamic forces and moments on the external aftbody fuselage and interfairing surfaces. The nozzle balances were instrumented to obtain the normal, side, and axial forces and pitching moment on the outer shell of each nozzle. Metallic bellows were installed in all balances to seal the gap between the metric and nonmetric balance segments. The rms error between indicated and applied axial balance loads, as determined from dead weight calibration results, is within 0.1% of design load for all installed force balances.

The two most important parameters measured during the twin-jet tests were aft-end (nozzle and aftbody fuselage and interfairing) drag and nozzle pressure ratio. The aft-end drag was calculated in two separate ways: 1) using the indicated balance forces and cavity pressures and 2) using the measured boundary layer rake and model surface pressures. The rms deviation in aft-end drag obtained from the two calculation methods is within four counts (one count equal to drag coefficient of 0.0001). The corresponding mean deviations are within one count, indicating little bias or systematic error. Better agreement would be difficult to obtain since the balance results are repeatable to within an rms value of three counts.

The nozzle pressure ratio was calculated from one-dimensional flow relationships using the venturi meter air-flow rate and the flow tube average static pressure, total temperature, and cross-sectional area for the faired-over inlet models and from the flow tube total pressure rake for the flow-through inlet models. A single total pressure probe at the centerline of the flow tube was used for monitoring and setting the nominal exhaust flow conditions.


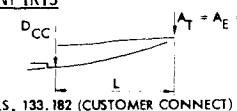
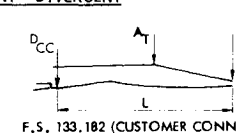
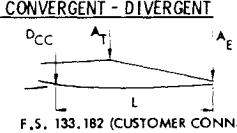
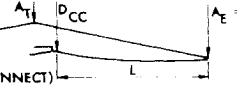
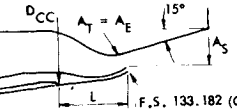
Jet-Effects Model Data

Nozzle Type and Power Setting Effects

The effects of nozzle type and power setting on aft-end drag coefficients and nozzle thrust and discharge coefficients were derived from comparisons in which only the nozzle model was varied. The nozzle configurations investigated during the program are identified in Table 1. The external contours of all basic nozzle configurations were designed to mate with a fixed diameter circular opening (eight-inch diameter in model scale) and a seven-degree surface angle at the aftbody/nozzle junction (designated as the customer connect station). Alternate convergent-divergent nozzles were fabricated in order to determine the effect of nozzle axial position on aft-end pressure distributions and drag. The alternate nozzles had the same contours as the basic nozzles, but were moved forward 3.802 in. with respect to the model aftbody.

Aft-end drags for all nozzle types tested at Mach 0.9 are presented in Fig. 5 as a function of nozzle throat area (normalized by the metric break area). The convergent-divergent nozzle has the lowest drags except at maximum

Table 1 Nozzle configuration identification

NOZZLE TYPE	NOZZLE POWER SETTING	IDENTIFICATION SYMBOL	GEOMETRIC PARAMETERS			
			A_E/A_T	A_S/A_T	A_S/A_{CC}	L/D_{CC}
CONVERGENT FLAP 	NORMAL	CF_1	1.0	1.0	0.252	0.512
	MAX A/B	CF_3	1.0	1.0	0.529	0.461
CONVERGENT IRIS 	NORMAL	CI_1	1.0	1.0	0.252	0.828
	MAX A/B	CI_3	1.0	1.0	0.529	0.552
CONVERGENT - DIVERGENT 	NORMAL	CD_1	1.10	1.10	0.278	1.012
	PARTIAL A/B	CD_2	1.22	1.22	0.471	1.023
	MAX A/B	CD_3	1.60	1.60	0.846	1.027
ALTERNATE CONVERGENT - DIVERGENT 	NORMAL	CD_{1A}	1.10	1.10	0.278	0.536
	MAX A/B	CD_{3A}	1.60	1.60	0.846	0.552
CONVERGENT - DIVERGENT EJECTOR 	MAX A/B	CDE_3	2.14	2.14	1.131	0.695
UNSHROUDED PLUG 	NORMAL	UP_{A1}	1.0	2.38	0.601	0.439
	PARTIAL A/B	UP_{A2}	1.0	1.83	0.733	0.441
	MAX A/B	UP_{A3}	1.0	1.67	0.870	0.439

A/B , and the unshrouded plug nozzle, which has little external flow recompression on the aft-end, has the highest. The drag decrease from normal to maximum A/B power settings is smaller for the convergent-divergent and convergent iris nozzles than for the other nozzle types. The long smooth external contours of the convergent-divergent and convergent iris nozzles at normal power allow greater exhaust pressurization of the boattail surface; this effect disappears as the nozzle throat area increases and the boattail projected frontal area decreases. The external contours of the unshrouded plug, convergent flap, and alternate convergent-divergent nozzles become smoother and lose projected frontal area as the nozzle throat area increases, resulting in significantly lower drag at maximum A/B than at normal power.

At supersonic speeds, the aft-end drags are highest for the normal power convergent-divergent and convergent iris nozzles, which have the greatest projected area, and decrease with increasing nozzle throat area (decreasing boattail projected area) for all nozzle types investigated. Drag differences between nozzle types are small at maximum A/B .

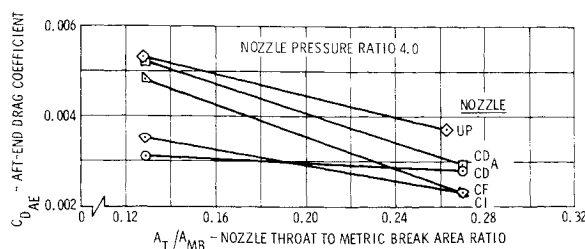


Fig. 5. Effect of nozzle type and power setting on aft-end drag - Mach 0.9

Nozzle Plume Simulation Effects

An investigation into the feasibility of simulating nozzle exhaust plume effects on aft-end drag by using solid-plume shapes was conducted. The following three solid body shapes were used to simulate the maximum A/B convergent iris nozzle plume: 1) a sting of cross-sectional area slightly over half of the nozzle exit area, roughly representative of jet-off conditions, 2) a cylindrical body the same diameter as the nozzle exit, representative of choked pressure ratio operation, and 3) a plume-shaped body designed to simulate the nozzle exhaust plume shape at nozzle pressure ratios greater than that required for choked operation.

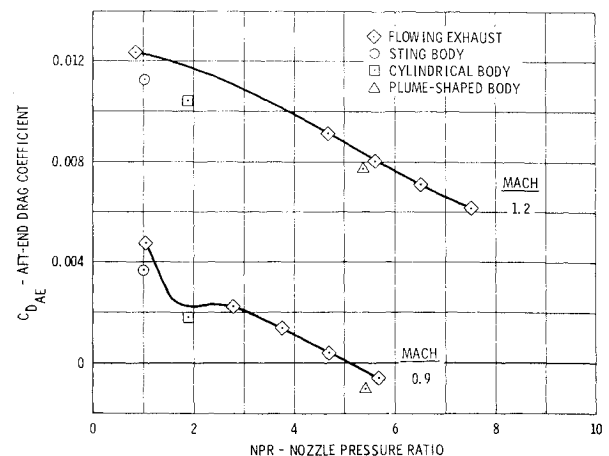
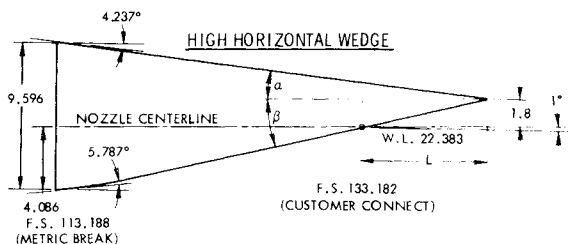
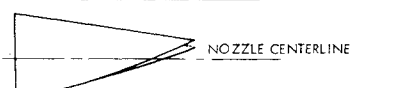
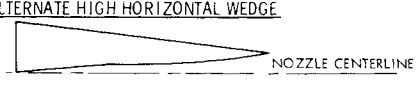
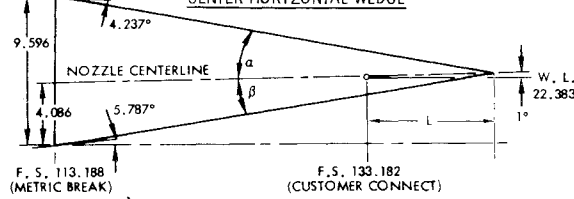
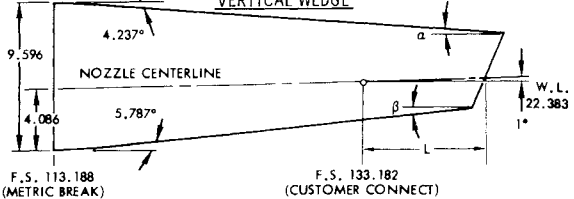
Fig. 6 Effect on nozzle plume simulators on aft-end drag - CI_3 nozzle.

Table 2 Interfairing configuration identification

INTERFAIRING TYPE	INTERFAIRING LENGTH, L INCHES	IDENTIFICATION SYMBOL			TRAILING EDGE ANGLE - DEGREES	
		NOZZLE SPACING RATIO, S/D			α	β
		1.25	1.625	2.0		
 <p>HIGH HORIZONTAL WEDGE</p>	0	N1B	I1B	W1B	10.792	19.683
	3.5	N1C	I1D	W1D	9.091	15.508
		N1D/C			7.519	12.339
	8.216	N1D	I1D	W1D	7.519	12.339
		N1E/D			6.450	10.385
 <p>MODIFIED HIGH HORIZONTAL WEDGE</p>	0		I4B		10.792	19.683
 <p>ALTERNATE HIGH HORIZONTAL WEDGE</p>	0			W4B	10.792	8.37
	8.216			W4D	7.519	6.80
 <p>CENTER HORIZONTAL WEDGE</p>	-4.0		I2B	W2A	23.061	17.202
	0			W2B	16.688	12.412
	3.5			W2C	13.788	10.237
	8.216		I2D	W2D	11.243	8.347
	13.0			W2E	9.58	7.106
 <p>VERTICAL WEDGE</p>	8.216	N3D			5.25	4.75
		N3E/D			5.25	4.75
	13.0	N3E			90.00	90.00

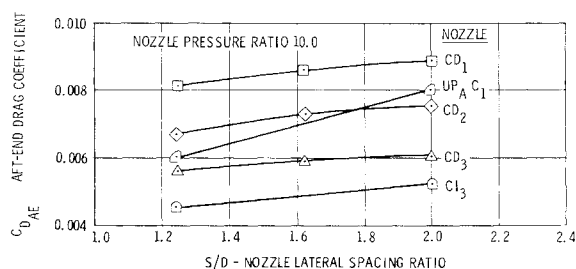


Fig. 7 Effect of nozzle lateral spacing on aft-end drag - Mach 1.6.

The results of the study, which are shown in Fig. 6, indicate that the total aft-end drags are lower for all three simulations than those of the flowing exhaust model. The sting body data in Fig. 6 were plotted at a pressure ratio of one, and the cylindrical body data were plotted at the choked nozzle pressure of 1.89. The plume-shaped body data were plotted at the pressure ratio of 5.4. This is the average pressure ratio at which the local expansion of the exhaust flow to the measured nozzle base pressure at the nozzle exit yields a plume slope equal to that of the plume-shaped fairing. Since the sting fills only slightly over half the nozzle exit, it might be expected to have less drag than the jet-off nozzle due to the reduced base area. The solid body simulations of jet-on conditions provide the drag-decreasing "following body" effect of a flowing exhaust (i.e., increases of the static pressures on the boat-tail in the trailing edge region) but not the drag-increasing pumping effect of the external flow.

Nozzle Lateral Spacing Effects

The effects of nozzle lateral spacing on aft-end and forebody drag forces were determined for alternate narrow-spaced and wide-spaced fuselage configurations which have the same cross-sectional area distribution as the basic intermediate-spaced fuselage configuration. The maximum fuselage area for the basic fuselage configuration increases with increasing spacing since the interfairing width for a given profile also increases. For the alternate narrow-spaced fuselage configurations, area was added to the side of the basic narrow-spaced fuselage centerbody and aftbody so that the desired area distribution could be achieved by using the basic interfairings. For the alternate wide-spaced fuselage configurations, area was removed from the side and bottom surfaces of the basic wide-spaced fuselage centerbody and from the lower surface of the interfairings.

An increase in nozzle lateral spacing results in a slight decrease in aft-end drag at subsonic speeds and a significant increase at supersonic speeds. The slight drag reduction at subsonic speeds (approximately 3 counts) is approximately equally split between reduced aftbody and nozzle boattail drags. The drag increase at supersonic speeds, illustrated by the Mach 1.6 data presented in Fig. 7, is due to a reduction in the extent of flow separation as the nozzle spacing increases.

An increase in nozzle lateral spacing reduces the aircraft model forebody drag, as determined from the airframe balance, by about eight counts at Mach 0.6 and increases the forebody drag by about 28 counts at Mach 1.6.

Since a four degree rudder deflection to the right as viewed looking forward causes the right-hand nozzle drag with the normal power convergent-divergent nozzles in-

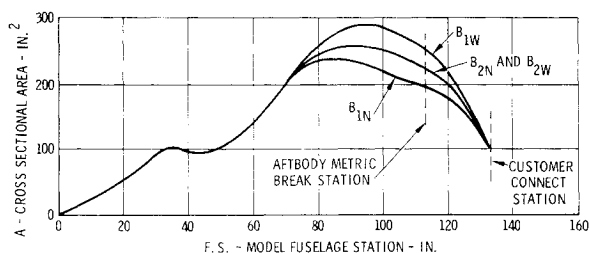


Fig. 11 Aircraft model area distributions.

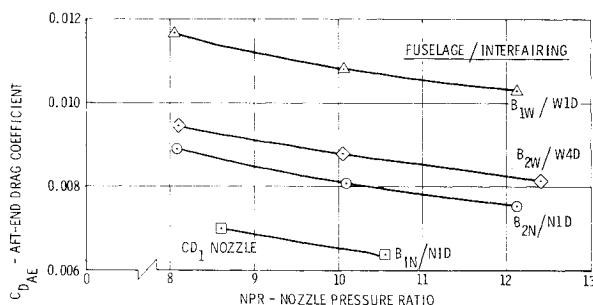


Fig. 12 Effect of fuselage area distribution on aft-end drag - Mach 1.6.

stalled to decrease and the left-hand nozzle drag with the normal power unshrouded plug nozzles installed to increase, little change in aft-end drag with rudder deflection is expected. However, this conclusion cannot be substantiated since no nozzles were tested with active nozzle balances on both sides of the model.

Fuselage Area Distribution Effects

The effects of fuselage area distribution on the aft-end and forebody drags were determined for the basic and alternate narrow-spaced fuselage configurations (designated B_{1N} and B_{2N} , respectively) and the basic and alternate wide-spaced fuselage configurations (designated B_{1W} and B_{2W} , respectively). The fuselage cross-sectional area distributions for these configurations are presented in Fig. 11. The data from the alternate narrow-spaced and wide-spaced fuselage configurations were used previously in determining nozzle lateral spacing effects.

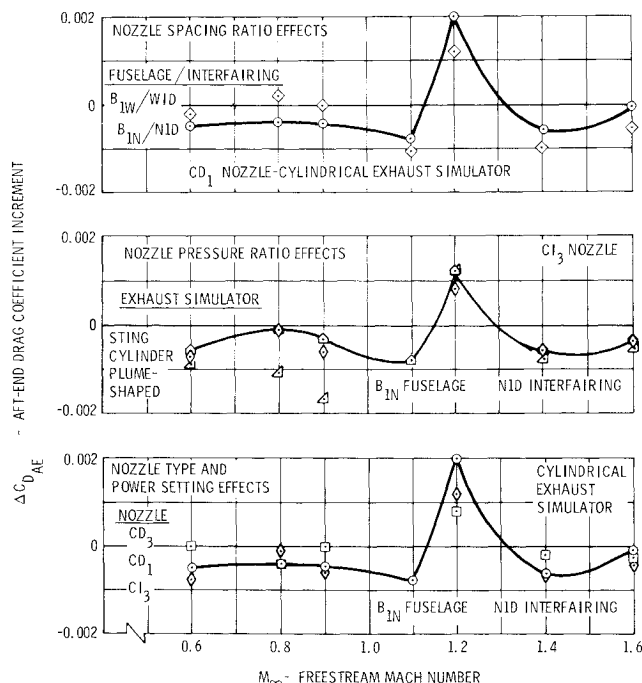


Fig. 13 Effect of strut interference on aft-end drag.

The aft-end drag of the alternate narrow-spaced fuselage configurations is slightly greater than that of the basic narrow-spaced configurations at subsonic speeds and substantially higher at supersonic speeds, as illustrated by the Mach 1.6 data presented in Fig. 12. This higher drag is due to both the larger projected frontal area of the alternate configurations and the associated larger magnitude negative pressure coefficients on the aft-facing surfaces. The forebody drag of the alternate configurations is approximately the same as that of the basic configurations since the difference in the sum of forward and aft-facing projected frontal areas is only 10 in.²

The aft-end drag of the basic wide-spaced fuselage configurations is approximately 7 counts greater than that of the alternate narrow-spaced configurations at subsonic speeds and significantly higher at supersonic speeds, as illustrated by the Mach 1.6 data in Fig. 12. The higher drag of the basic configurations is due to both a higher Mach number at the metric break station and a larger projected frontal area. At subsonic speeds, no consistent forebody drag trend was observed. At supersonic speeds, however, the forebody drag of the basic configurations is consistently about 14 counts higher than that of the alternate configurations. The forebody drag increase for the basic configurations is due to a 50 in.² larger sum of forward and aft-facing projected frontal areas.

Model to Aircraft Drag Corrections

Strut Interference Effects

The effects of strut interference on aft-end drag were determined by testing the model with a twin-sting support, which stimulates the nozzle exhaust plumes, and with a strut support in combination with a dummy twin-sting arrangement. In order to isolate the strut interference effect, the dummy stings were designed to duplicate a sufficient portion of the load-carrying sting geometry so that both types of stings would have the same influence on aft-end drag, as determined from potential flow analysis results. The achievement of this design objective was confirmed during the wind-tunnel test when no significant difference in nozzle drag was obtained when a wedge fairing was both installed and removed from the dummy stings. This fairing was similar to the one used to connect the twin load-carrying model stings to the single tunnel sting/strut support. Both types of stings were designed to simulate the nozzle exhaust plumes so that the aft-end geometry would represent, as closely as possible, an actual aircraft installation.

Since aft-end drag increments are generally applied to a reference aircraft model drag in a conventional accounting system, the variation of strut interference drag with nozzle power setting and exhaust plume shape was investigated for several nozzle types and lateral spacings. As shown in Fig. 13, strut interference effects on aft-end drag are 10 drag counts or less at all test Mach numbers except 0.9 and 1.2, where the interference effects are up to 20 drag counts. Strut interference causes lower aft-end drag forces at all test Mach numbers except 1.2, where the strut interference effects are unfavorable. The favorable interference effects increase with increasing nozzle boat-tail angle and exhaust plume size and are larger for the narrow-spaced configurations than for the wide-spaced configurations at subsonic speeds and smaller at supersonic speeds.

Inlet Spillage Effects

Inlet spillage corrections for different nozzle power setting positions and lateral spacings were determined by comparing the aft-end drag obtained for faired-over inlet configurations with that obtained for the flow-through

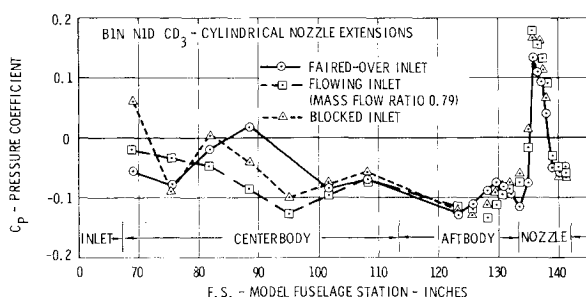


Fig. 14 Effect of inlet spillage on bottom centerbody/afterbody/nozzle pressure distributions - Mach 1.6.

inlet configurations operating at the inlet mass ratio required by the aircraft. Mass flow ratios near unity were obtained by providing an unblocked flow area from the cowl lip to the nozzle exit. Reduced inlet mass flow ratios were created by providing orifice plates within the model. Cylindrical extensions were attached to the nozzles so that inlet spillage effects on aft-end drag could be isolated from nozzle pressure ratio effects.

The effects of inlet mass flow ratio and inlet geometry at zero mass flow ratio on aft-end drag are within 5 drag counts for all configurations examined. The aft-end drag is slightly lower for the faired-over inlet model than that for the blocked inlet model at subsonic speeds and slightly higher at supersonic speeds. A slight rise in drag at the higher mass flow ratios occurs for the narrow-spaced configurations. As shown by the pressure distributions in Fig. 14, the inlet disturbances diminish as they propagate aft and have little effect on the aft-end drag of the model tested.

Wing and Stabilizer Span Reduction Effects

Tests were conducted with and without the wing installed on the aircraft model and with stabilizers of different span to determine the effects of these changes on aft-end drag.

The aft-end drag increases by approximately 8 drag counts when the wing is removed at subsonic speeds and decreases by about the same amount at supersonic speeds. The presence of the stabilizers makes little difference in the drag increment due to the wing.

The effects of stabilizer span reduction on aft-end drag can be significant at subsonic speeds, as shown in Fig. 15, and are negligible at supersonic speeds. The changes from partial to short span and from short span to fuselage fairing alone result in significant reductions in aft-end drag at subsonic speeds. Little effect is evident for stabilizer span reduction from full to partial span or from fuselage fairing alone to no stabilizer and no fairing.

Reynolds Number Effects

As would be expected from considerations of skin friction drag trends, the aircraft drag coefficient decreases with increasing Reynolds number. The aircraft pressure drag coefficient, however, increases with increasing Rey-

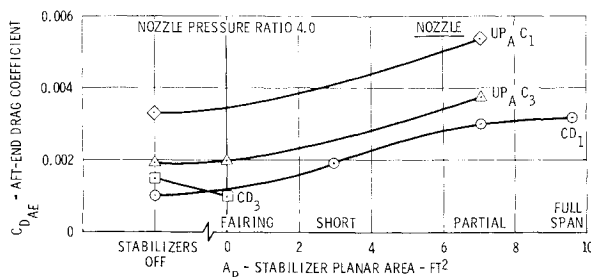


Fig. 15 Effect of stabilizer span reduction on aft-end drag - Mach 0.9.

nolds number with most of the increase occurring on the aft-end portion of the aircraft. The aircraft drag coefficients were obtained from force balance data, and the aircraft pressure drag coefficients were obtained by subtracting the calculated skin friction drag coefficient from the measured values.

The aft-end drag coefficient trend within the Reynolds number range tested is just the opposite of that for the aircraft. As shown by the Mach 0.9 data presented in Fig. 16, the aft-end drag coefficient increases at a decreasing rate with increasing Reynolds number, even though the friction component of the drag coefficient decreases. At Reynolds numbers equal to or greater than the basic test Reynolds number of 2.5 million per foot, the change in aft-end drag coefficients is small and within the accuracy of the force balance data. An examination of aft-end pressure data indicates that most of the Reynolds number effect occurs on the initial part of the aftbody and almost no effect exists within the recompression region near the nozzle exit. The Reynolds number effects were approximately the same for both the strut-supported and sting-supported models.

Conclusions

The best aft-end design examined during the program, as determined by using the measured jet-effects model data in conducting mission analysis studies for seven selected configurations, consists of convergent-divergent nozzles, a high horizontal wedge interfairing with the trailing edge at the nozzle exit, a single vertical stabilizer, and a narrow nozzle lateral spacing. The mission radii for a fixed aircraft TOGW (takeoff gross weight) of 45,000 lbs was 35% less for the worst configuration, which was still a realistic design, than that for the best configuration for a subsonic air superiority mission and as much as 50% less for a supersonic point intercept mission.

Since the aircraft mission radii can be significantly affected by aft-end design changes and the aft-end drag associated with the reference aircraft model is generally small due to shallow boattail angles, the aft-end drag increment obtained from the jet-effects model data must be accurately determined early in the aircraft design cycle. Sufficient jet-effects model data should be obtained so that nozzle power setting and pressure ratio effects on aft-end drag can be determined for all flight conditions within the mission envelope. If equivalent body techniques are used to calculate the reference aircraft model drag, then an aft-end drag increment must be determined to account for twin-nozzle/aftbody/stabilizer interaction effects.

The lack of aircraft flowfield simulation, as related to strut interference, inlet spillage, wing and stabilizer span reduction, and tunnel Reynolds number, can have a significant effect on aft-end drag. Although these effects tended to cancel in the computation of the aft-end drag increments for the twin-jet model of this program, such a situation may not exist for other models, especially ones of smaller scale with large separated flow regions, closely coupled inlet/nozzles systems, and a support strut located near the aft-end portion of the aircraft. As a result, aircraft flowfield simulation effects on jet-effects model data

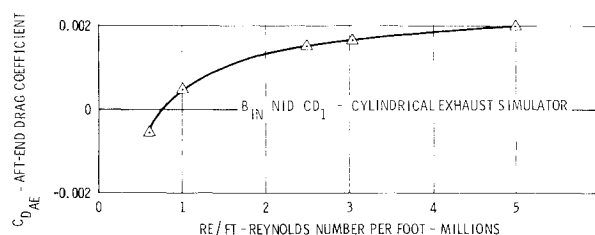


Fig. 16 Effect of Reynolds number on aft-end drag - Mach 0.9.

should be investigated during the aircraft design cycle, even if larger scale models with less flowfield simulation are utilized initially.

References

- ¹Glasgow, E. R., Santman, D. M., and Miller, L. D., et al., "Integrated Airframe-Nozzle Performance for Designing Twin-Engine Fighters," AFFDL-TR-73-71, June 1973, Air Force Flight Dynamics Lab., Wright-Patterson Air Force Base, Ohio.
- ²Galigher, L. L., "Integrated Airframe Nozzle Performance Characteristics of a Generalized Twin-Jet, Air Superiority Fighter Aircraft Model at Mach Numbers From 0.6 to 1.6," AEDC-TR-73-125, July 1973, Arnold Engineering Development Center, Tullahoma, Tenn.
- ³Glasgow, E. R., Santman, D. M., and Miller, L. D., et al., "Experimental and Analytical Determination of Integration Air-

frame-Nozzle Performance," AFFDL-TR-72-101, Oct. 1972, Air Force Flight Dynamics Lab., Wright-Patterson Air Force Base, Ohio.

⁴Presz, W., "Experimental and Analytical Determination of Integrated Airframe-Nozzle Performance, Phase III Summary Report, Pratt & Whitney Aircraft Support Program," PWA-4503, July 1972, Pratt and Whitney, East Hartford, Conn.

⁵Glasgow, E. R., Divita, J. S., Everling, P. C., and Laughrey, J. A., "Analytical and Experimental Evaluation of Performance Prediction Methods Applicable to Exhaust Nozzles," AIAA Paper 71-719, Salt Lake City, Utah, 1971.

⁶Glasgow, E. R. and Santman, D. M., "Aft-End Design Techniques for Twin-Engine Fighters," *Journal of Aircraft*, Vol., No. 1, Jan. 1974, pp. 39-44.

⁷General Dynamics/Fort Worth Division, "Supersonic Inlet Design and Airframe-Inlet Integration Program (Project Tailor-Mate)," AFFDL-TR-71-124, May 1973, Air Force Flight Dynamics Lab., Wright-Patterson Air Force Base, Ohio.

JUNE 1974

J. AIRCRAFT

VOL. 11, NO. 6

Engineering Notes

ENGINEERING NOTES are short manuscripts describing new developments or important results of a preliminary nature. These Notes cannot exceed 6 manuscript pages and 3 figures; a page of text may be substituted for a figure and vice versa. After informal review by the editors, they may be published within a few months of the date of receipt. Style requirements are the same as for regular contributions (see inside back cover).

Vortex Measurements Behind a Swept Wing Transport Model

K. L. Orloff* and D. L. Ciffone†

NASA Ames Research Center, Moffett Field, Calif.

Introduction

A CONSIDERABLE amount of information documenting the structure of aircraft wake turbulence has been produced over the last several years. Quantitative detailing of the flow has, however, been primarily restricted to wings with simple near-rectangular or elliptic span loadings. The need for experimental velocity distributions from models of wings representative of today's modern transport aircraft is the rationale for the measurements being reported.

A backscatter laser Doppler velocimeter (LDV) which simultaneously senses two components of the velocity (axial and tangential), has been used to traverse and measure the velocity distributions in the near wake of a swept wing semi-span transport model in the NASA-Ames 7- by 10-foot wind tunnel.¹ This LDV instrument has previously been used to measure the velocity distributions in the wake of a rectangular airfoil.^{2,3,4} The model configuration included nacelles, pylons, anti-shock bodies, and wing flaps which could be deflected 27°. Further details of this semispan wing model are available in Ref. 5.

Apparatus and Procedure

The semispan model was mounted vertically from the floor of the wind tunnel. The test Reynolds number per meter was nominally 1.24×10^6 . Since the LDV system was restricted to the location of the optical window, the

wing model was placed in a forward position in the test section to allow data to be obtained at the maximum aft location $x/b = 1.25$ where x is distance measured downstream from the wing tip and b is the wing span ($b/2 = 91.5$ cm.). Data were also obtained at $x/b = 0.49$, and a full study was made of the streamwise dependence of the velocity fields with changes in wing configuration.¹ At each location both the LDV measuring station and the model position were well within the test section to insure flow uniformity.

LDV scanning was performed in a direction normal to the tunnel centerline, with the upper wing surface closest to the window through which the measurements were taken. The complication of vortex movement within the test section has been overcome as a result of the spatial scanning capability of the laser velocimeter. The Doppler information was processed on two separate spectrum analyzer systems as the focal point of the velocimeter was continuously traversing the vortex. The scan automatically reversed at end limits which were preset to contain the flow area of interest. Full details on signal processing, data acquisition, and core identification are given in Refs. 1, 2, and 3.

Velocity distributions are presented as fractions of free-stream velocity, U , and location Z , relative to the trailing edge ($Z = 0$), normalized by the span, b . A positive value for Z/b indicates a location on the side below the wing planform.

Results and Discussion

Typical wake vortex velocity profiles are presented in Figs. 1 and 2 for the flaps-retracted and the flaps-deployed 27° configurations, respectively. It can be seen that the repeatability of the data for different traverses is excellent, and the vortex structure can be accurately defined. The data show a slightly higher axial velocity defect for the flaps-deployed configuration, but no perceptible change in the maximum tangential velocity. While deployment of the flaps increases the total circulation [which should increase $(V_0/U_\infty)_{\max}$], it also alters the lift distribution, moving the center of vorticity inboard along

Received December 3, 1973; revision received April 5, 1974.

Index categories: Jets, Wakes, and Viscid-Inviscid Flow Interactions; Aircraft Aerodynamics (Including Component Aerodynamics).

*Research Scientist. Member AIAA.

†Research Scientist.